Flight calibration of the Suzaku XIS using the charge injection technique

Citation: Ozawa, Midori et al. "Flight calibration of the Suzaku XIS using the charge injection technique." Space Telescopes and Instrumentation 2008: Ultraviolet to Gamma Ray. Ed. Martin J. L. Turner & Kathryn A. Flanagan. Marseille, France: SPIE, 2008. 70112B-12. © 2008 SPIE

As Published: http://dx.doi.org/10.1117/12.788258

Publisher: Society of Photo-Optical Instrumentation Engineers

Persistent URL: http://hdl.handle.net/1721.1/52634

Version: Final published version: final published article, as it appeared in a journal, conference proceedings, or other formally published context

Flight calibration of the Suzaku XIS using the charge injection technique

Midori Ozawa[a], Hideki Uchiyama[a], Hiroshi Nakajima[b], Hideyuki Mori[a], Hironori Matsumoto[a] ,Takeshi Go Tsuru[a], Katsuji Koyama[a], Masahiro Uchino[b], Kiyoshi Hayashida[b], Hiroshi Tsunemi[b], Hiroshi Murakami[c], Tadayasu Dotani[d], Gregory Prigozhin[e], Steve Kissel[e], Eric Miller[e], Beverly LaMarr[e] and Marshall Bautz[e]

[a] Department of Physics, Kyoto University, Kita-Shirakawa, Sakyou-ku, Kyoto, Japan;
[b] Department of Earth and Space Science, Osaka University, Machikane-yama, Toyonaka, Osaka, Japan;
[c] Department of Physics, Rikkyo University, 3-34-1 Nishi-Ikebukuro,Toshima,Tokyo, Japan;
[d] Institute of Space and Astronautical Science, Japan Aerospace Exploration Agency, Yoshino-dai, Sagamihara, Kagawa, Japan;
[e] Kavli Institute for Astrophysics and Space Research, Massachusetts Institute of Technology, Cambridge, MA, USA

ABSTRACT

The X-ray Imaging Spectrometer (XIS) on board the Suzaku satellite is an X-ray CCD camera system that has features of a low background, high quantum efficiency, and good energy resolution in the 0.2–12 keV band. Because of the radiation damage, however, the energy resolution of the XIS has been degraded since Suzaku was launched (July 2005). In order to improve the energy resolution, one of the major advantages of the XIS over the other X-ray CCDs in orbit is the provision of a precision charge injection (CI) capability. We applied this CI in two ways. First, in order to measure the precise charge transfer inefficiency (CTI), we applied the checker-flag CI, and measured the CTI of each CCD column. Furthermore, we obtained the pulse height dependency of the CTI. Our precise CTI correction using these results improved the energy resolution from 193 eV to 173 eV in FWHM at 5.9 keV in July 2006 (one year after the launch). Second, the energy resolution can be improved also by reducing the CTI. For this purpose, we applied the spaced-row charge injection (SCI); periodically injected artificial charges work as if they compensate radiation-induced traps and prevent electrons produced by X-rays from being captured by the charge traps. Using this method, the energy resolution improved from 210 eV to 150 eV in FWHM at 5.9 keV in September 2006, which is close to the resolution just after the launch (140 eV). We report the current in-orbit calibration status of the XIS data using these two techniques. We present the time history of the gain and energy resolution determined from onboard calibration sources (^{55}Fe) and observed calibration objects like E0102–72.

Keywords: X-ray, CCD, charge injection, Suzaku satellite

1. INTRODUCTION

After the first successful space flight use of X-ray Charge Coupled Device (CCD) of the SIS units (Burke et al. 1993[1]) on board ASCA, the CCD has been playing a major role in imaging spectroscopy of X-ray astronomy. However, the gain and energy resolution of X-ray CCDs in orbit degrade due to an increase of the charge transfer inefficiency (CTI). This is because the irradiation of charged particles makes the charge traps, and these traps capture some portion of the charge through the transfer. The CTI is defined as the ratio of lost charge to transferred charge in one transfer.

Further author information: (Send correspondence to M.O.)
M.O.: E-mail: midori@cr.scphys.kyoto-u.ac.jp, Telephone: 81 75 753 3869

Space Telescopes and Instrumentation 2008: Ultraviolet to Gamma Ray, edited by Martin J. L. Turner, Kathryn A. Flanagan, Proc. of SPIE Vol. 7011, 70112B, (2008) · 0277-786X/08/$18 · doi: 10.1117/12.788258

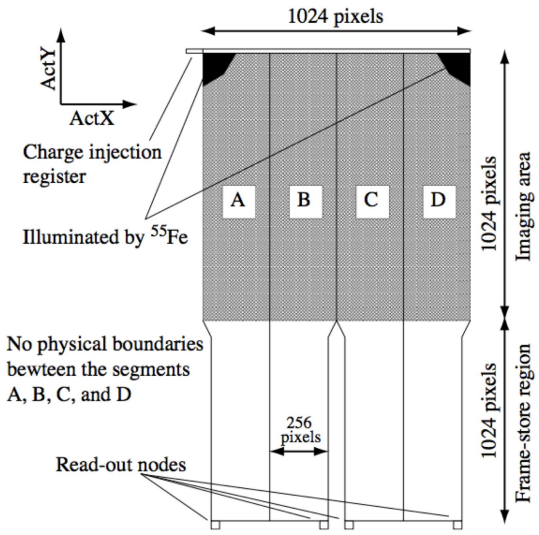

Figure 1. Schematic view of the XIS CCD (FI chip). In order to inject a charge packet, a serial register is equipped at the top of the imaging area. The chip has four readout nodes, one for each segment. Signals are simultaneously read from these nodes. For the BI chip, the charge-injection register runs from segment D to A. This figure is adopted from Koyama et al. (2007).[7]

The X-ray Imaging Spectrometer (XIS) on board the Japanese fifth X-ray satellite, Suzaku,[6] had high-energy resolution, ∼140 eV (FWHM) at 5.9 keV, in August 2005, just after the first light, but the resolution degraded to ∼210 eV (FWHM) by August 2006. In order to mitigate the effect of radiation damage, the XIS is equipped with a charge injection (CI) structure[3–5] which can inject a commandable quantity of charge in a nearly arbitrary spatial pattern.

The CI can be used in two ways. First, we can measure the CTI of each column precisely by the checker-flag CI technique.[10] Second, we inject charge packets into the CCD rows periodically and reduce the CTI. The injected charge works as if it compensates radiation-induced traps and prevents the traps from capturing an X-ray signal charge. This method is called the spaced-row charge-injection (SCI) technique. Results of ground experiments using the SCI technique with radiation-damaged CCDs have been reported.[2,4] The Suzaku XIS started the SCI technique in orbit in August 2006.

Hereafter, we call the data with the SCI technique "SCI-on data", and those without the SCI technique "SCI-off" data. All data with the observation date before July 2006 are the SCI-off data, and those after May 2007 are all SCI-on data except for some calibration observations. In this paper, all errors are at the 1σ confidence level unless mentioned.

2. SUZAKU XIS

Koyama et al. (2007)[7] have provided details on the XIS. Here, we briefly summarize relevant instrument characteristics. The CCDs are MOS-type with three-phase frame transfer. There are four CCDs on board Suzaku; three are front-illuminated (FI) chips (XIS 0, 2, and 3) and one is a back-illuminated (BI) chip (XIS 1). The XIS 2 CCD chip became unusable in November 2007. Although the reason has not been identified, we consider it is most likely due to a micro-meteorite attack.

Figure 1 is a schematic view of the XIS CCD. The imaging area of the CCD has 1024 × 1024 pixels. The pixel size is 24 μ m × 24 μ m, giving a size of 25 mm × 25 mm for the imaging area. Two calibration sources (^{55}Fe) illuminate the two far-end corners from the read-out node of the imaging area.

A position in the imaging area is defined by the detector-fixed coordinates ($ActX$, $ActY$), where the origin (0,0) is taken to be the first pixel read-out of segment A in the normal clocking mode. In the imaging area, $ActX$

Table 1. Log of the checker-flag charge-injection experiments in orbit.

Date	Total effective exposure	The equivalent X-ray energy of the injected charge packets (keV)			
	(ksec)	XIS0	XIS1	XIS2	XIS3
2006/1/20	3.7	-	6.6	-	4.4
2006/5/21	1.2	4.0	-	3.7	-
2006/6/26	4.9	-	0.3/6.8	-	0.5/4.4
2006/7/17	5.7	0.6/4.2/8.0	-	0.6/3.8/7.7	-
2006/8/25	4.9	-	0.3/6.8	-	0.5/6.6
2007/9/28	2.5	0.6/4.2/7.9	0.3/6.5/7.1	-	0.5/4.3/6.2

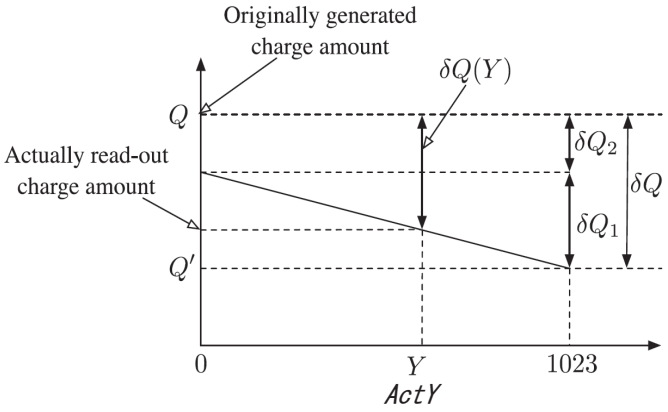

Figure 2. Phenomenological relationship between the charge amount of Q and the charge loss of δQ. δQ_1 and δQ_2 are the lost amount of charge through the slow transfer and fast transfer, respectively. This figure is adopted from Nakajima et al. (2008).[10]

runs from 0 to 1023 (from segment A to D), while $ActY$ runs from 0 to 1023 (from the read-out node to the charge injection register).

The charge injection structure lies adjacent to the topmost row of the imaging area. A detailed description of the charge injection structure and its electrical performance are presented in Prigozhin et al. (2004).[3] A detailed description of the performance of the charge injection capability of the Suzaku XIS is presented in Nakajima et al. (2008).[10] In Nakajima et al. (2008),[10] the results of the checker-flag CI is mainly based on ground-based experiments and in-orbit ones within a year after the launch. We can inject charges from ~ 50 e^- to ~ 4000 e^- per pixel; the equivalent X-ray energies range from $\sim$300 eV to $\sim$15 keV.

3. IN-ORBIT CALIBRATION OF SCI-OFF DATA

3.1 Checker-flag Observation and CTI Correction for SCI-off Mode

The CTI has increased since the launch due to the irradiation of charged particles in orbit. This increase of CTI causes several problems. First, it causes the $ActY$ dependence of the energy gain. Second this $ActY$ dependence of the gain causes the degradation of the energy resolution. Thus it is important to measure the CTI and correct the gain. Because the CTI is different from column to column, we can get more precise gain and energy resolution if we correct the CTI column by column. In the usual method, we use the ^{55}Fe calibration sources when measuring the CTI, and for this reason, we cannot obtain the CTI of every column. However, by performing the checker-flag CI experiments in orbit, we can measure the CTI of every column precisely. We briefly summarize how to get the column-to-column CTI .

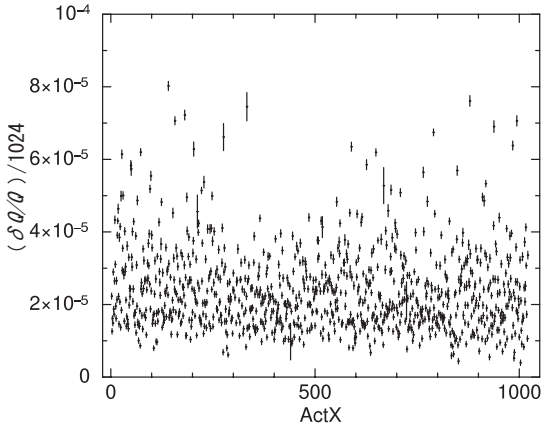

Figure 3. Distribution of the column-to-column CTI as a function of the *ActX* obtained through the checker-flag CI experiments. The equivalent X-ray energy of the injected charge packets is 4.2 keV. We show the CTI of XIS 0 in July 2006 as a typical example.

For the Suzaku XIS, the CTI is described as

$$Q' = (1 - CTI_{fast})^{1024} \cdot (1 - CTI_{slow})^{ActY} \cdot Q \sim (1 - 1024 \cdot CTI_{fast}) \cdot (1 - ActY \cdot CTI_{slow}) \cdot Q, \quad (1)$$

where Q and Q' represent an injected and a read-out amount of charge, respectively, while CTI_{fast} and CTI_{slow} represent the CTI with a fast transfer from the imaging area to the frame stored area, and that with a slow transfer after the fast transfer, respectively. We can use the approximation in the equation above, because the CTI is small (typically the order of 10^{-5}).

Figure 2 shows the relationship between the original amount of charge Q and the lost amount of charge $\delta Q = Q - Q'$. We define that the factor f is equal to $\delta Q_1/\delta Q$ in this figure, then we obtain

$$CTI_{slow} = (\delta Q_1/Q)/1024 = f \times CTI, \text{ and} \quad (2)$$
$$CTI_{fast} = (\delta Q_2/Q)/1024 = (1 - f) \times CTI, \quad (3)$$

where $CTI = (\delta Q/Q)/1024$, and δQ_1 and δQ_2 are the lost amount of charge in the slow transfer and the fast transfer, respectively. In the SCI-off mode, we assume $f = 0.4$ for the FI sensors and $f = 0.6$ for the BI sensor. These values were obtained using the method in figure 2 with the FeI Kα line from the Sgr C data in the Galactic center.

In the checker-flag CI, we can compare Q_{test} which is influenced by the CTI with Q_{ref} which is not influenced by the CTI because of the CI.[10] In the case of checker-flag CI, the $ActY$ of the injected charge is $\sim$1024. Considering Q_{ref} is Q (an injected amount of charge packets) and Q_{test} as Q' (a read-out amount of charge packets) in equation 1, we obtain

$$Q_{test} \sim (1 - 1024 \cdot CTI) \cdot Q_{ref}. \quad (4)$$

By measuring Q_{ref} and Q_{test} column by column, we can obtain the column-to-column CTI. The log of the checker-flag CI experiments in orbit is shown in table 1.

3.2 Result of Checker-flag CI Experiments in Orbit

First, we studied the distribution of the column-to-column CTI from the checker-flag CI experiments. The result is shown in figure 3. We can see that there is significant dispersion in the CTI of each column. Figure 4 indicates the time growth of the CTI is different between column and column.

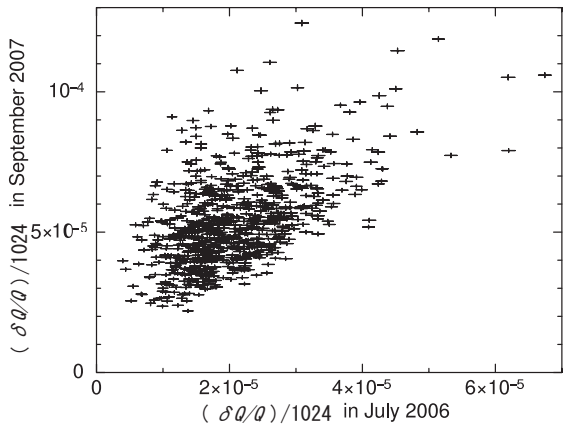

Figure 4. Time growth of the CTI of each column. Horizontal and vertical axes are the CTIs obtained from the checker-flag CI experiments in July 2006 and September 2007, respectively. The equivalent X-ray energy of the injected charge packets is 4.2 keV.

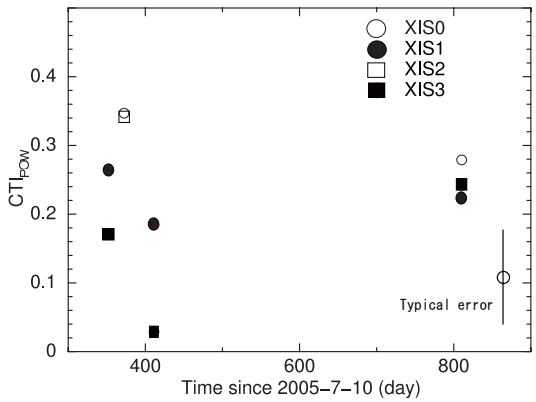

Figure 5. Time history of the power-index (CTI_{POW}) obtained from the checker-flag CI experiment. The CTI_{POW} is defined as $CTI \propto Q^{-CTI_{POW}}$, where Q is the injected charge.

Next, we show the relation between the CTI and the injected amount of charge. We assumed the CTI is expressed as[3]

$$CTI = CTI_{NORM} \times Q^{-CTI_{POW}}. \tag{5}$$

By injecting various amounts of charge, we can obtain CTI_{POW} and CTI_{NORM}. The time history of CTI_{POW} is shown in figure 5. Time averaged values of CTI_{POW} are 0.31, 0.22 0.34, and 0.15 for XIS 0, 1, 2, and 3, respectively. We will use these values in the CTI correction.

Thus, we obtained the CTI column by column. Also, by performing the checker-flag CI experiments several times, we obtained the time variability of the CTI column by column. Then we performed the column-dependent and time-dependent CTI correction. We show the results of the CTI correction in the following.

First, we checked the calibration sources (^{55}Fe). In figure 6, we compared the CTI correction methods; in the column-dependent CTI correction, we used the column to column CTI, while in the column-averaged CTI correction, each column of the same segment has the same CTI, which is equivalent to the segment averaged

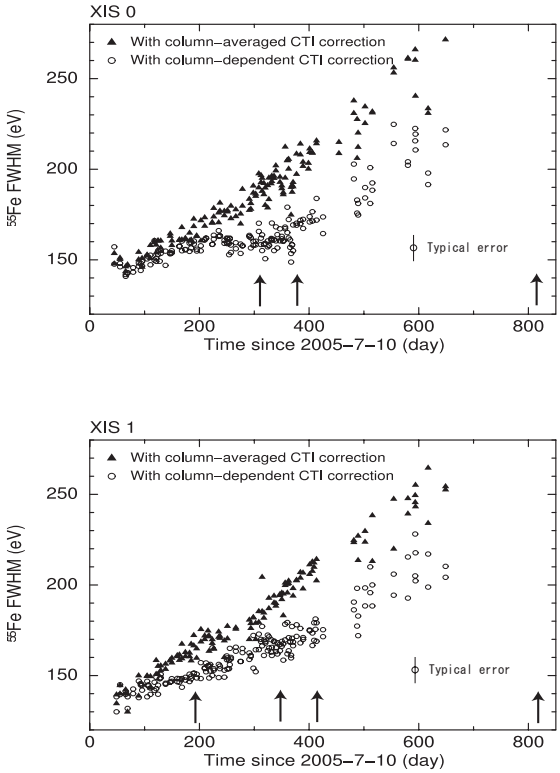

Figure 6. Time history of the energy resolution of MnI Kα line from the ^{55}Fe calibration sources for XIS 0 (upper panel) and XIS 1 (lower panel). The triangle and circle represent the data with the column-averaged and with the column-dependent CTI corrections, respectively. Note that the energy resolution becomes significantly better with the column-dependent CTI correction. Arrows in the plot indicate the days we performed the checker-flag CI experiments.

value of the column-dependent CTI. The energy resolution of MnI Kα line becomes significantly better with the column-dependent CTI correction than with the column-averaged CTI correction. Figure 7 shows the spectra which were observed in August 2006. We can clearly see the low-energy tail is reduced with the column-dependent CTI correction.

Second, we studied the data of Perseus cluster of galaxies to examine whether the CTI is corrected properly by checking the *ActY* dependence of the energy gain. The Perseus cluster of galaxies is one of the brightest clusters in X-ray. It has the X-ray spectrum of thermal plasma with the strong Kα line of FeXXV. The line center of the FeXXV Kα is almost spatially constant ($\sim$ 6.56 keV at z=0.0176), since its plasma temperature varies spatially between 4 keV and 7 keV. Its radius is $\sim 15'$ and can cover the entire field of view of the Suzaku XIS ($18' \times 18'$). Thus this source is suitable to measure the positional dependence of the gain caused by the CTI. We observed the Perseus cluster in February 2006 and August 2006. We divided the imaging area into four parts, each has the size of (*ActX*, *ActY*) = (1024, 256), and extracted spectra from these four parts. We fitted the spectra with a power-law model and a Gaussian function, and obtained the line center of FeXXV Kα for each part. Figure 8 shows the center energy of the FeXXV line as a function of *ActY*. The fact that there is no significant *ActY* dependence indicates that we estimated the CTI properly.

3.3 Time History of Gain and Energy Resolution

After the column-to-column CTI correction, we checked the energy gain using the data of ^{55}Fe and E0102–72. E0102–72 is one of the brightest supernovae remnants in the Small Magellanic Cloud. It looks as a point source considering the distance and the spatial resolution of Suzaku. It has many bright line emissions originated from

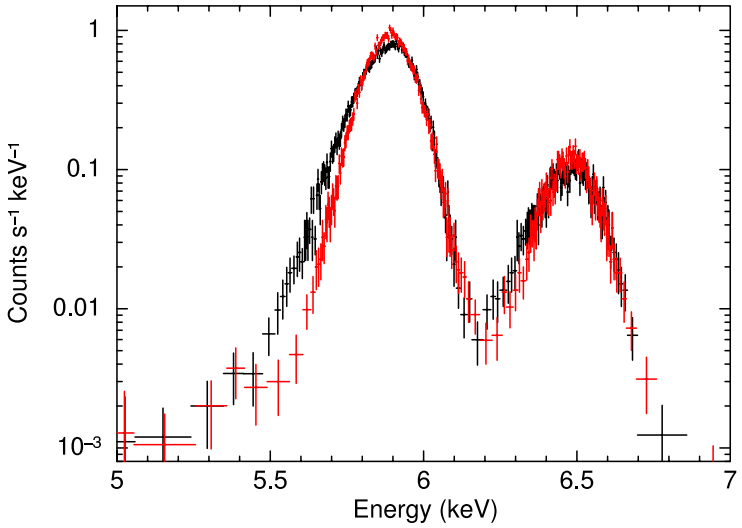

Figure 7. Energy spectra of the calibration source of segment D of XIS 2 in August 2006 with the column-averaged (black) and column-dependent (red) CTI corrections. Note that the low-energy tail component is significantly reduced with the column-dependent CTI correction.

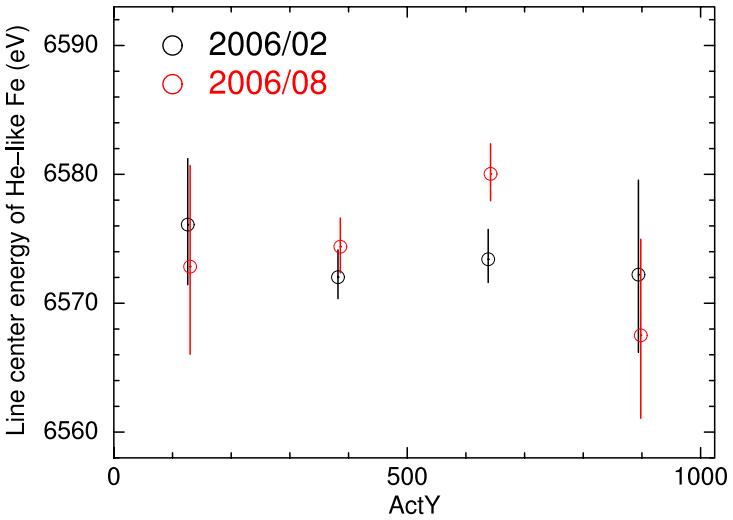

Figure 8. *ActY* dependence of the center energy of the Fe`XXV` line from the Perseus cluster. The black and red circles represent the observations in February 2006 and in August 2006, respectively.

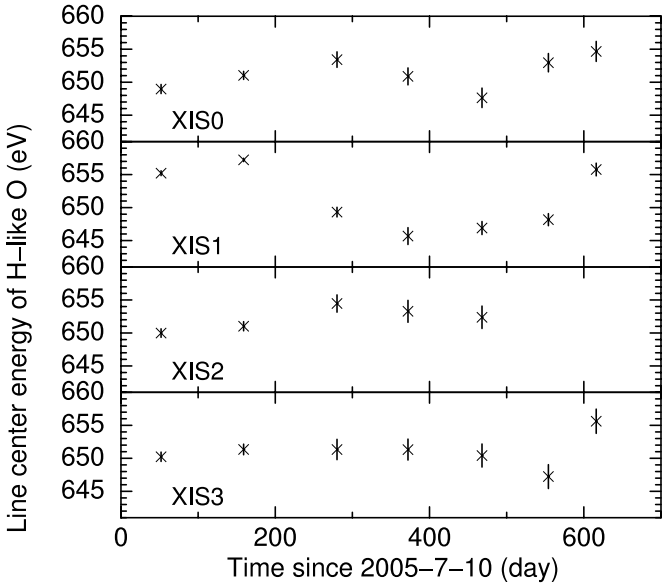

Figure 9. Time history of the center energy of the OVIII Kα line for XIS0-3 from the SCI-off data obtained in the E0102–72 observations.

thermal plasma, and an empirical model to describe the spectrum is established*. Thus, it is a good source to study a low-energy gain.

To begin with, we fine-tuned the charge-energy gain factor. This gain factor is determined as a conversion factor from the amount of charge to its equivalent X-ray energy. First, we studied the time history of the center energy of the MnI Kα line from the ^{55}Fe data. Although these data are CTI corrected, there remained a little time dependency of the energy gain. Thus, we fine-tuned the high-energy gain factor by multiplying a linearly time-dependent function. Then, we fine-tuned the low-energy gain factor using the time history of OVIII Kα line, NeIX Kα line, and NeX Kα line from the E0102–72 data.

After these fine-tunings, we rechecked the energy gain in order to examine we estimated the gain factor properly. First, we checked the E0102–72 data. Figure 9 shows the center energy of the OVIII line from the E0102–72 data after the CTI and the gain corrections. According to the empirical model, the center of OVIII Kα is $\sim$653 eV. Thus we can say the uncertainty of the absolute energy is $\pm$ 0.7 % at $\sim$0.65 keV. Second, we checked the ^{55}Fe data. Figure 10 shows the line center energy of the MnI Kα line; open circles indicate the SCI-off data. Each mark of the SCI-off data in the plot corresponds to an observation sequence whose effective exposure is more than 60 ksec. The theoretical line center energy of MnI Kα is 5895 eV. The uncertainty of the absolute energy is $\pm$ 0.1 % at $\sim$ 5.895 keV. Figure 11 shows the time history of the energy resolution of the MnI Kα line.

3.4 Response Function

The details of the energy response is described in Koyama et al. (2007).[7] We report the present calibration status of the response function. In order to model the time and energy dependence of the response, we used the SCI-off data of ^{55}Fe and E0102–72. We modeled the FWHM of the main peak component[7] as

$$FWHM = \sqrt{a(t) \times (E/5895)^{b(t)^2} + C(E)^2} \text{ (eV)}, \quad (6)$$

where *a(t)* is obtained from the time history of the line center energy of the MnI Kα, and *b(t)* is calculated from the energy resolutions of various lines from E0102–72. *C(E)* is a time-independent and energy-dependent

*http://cxc.harvard.edu/acis/E0102/

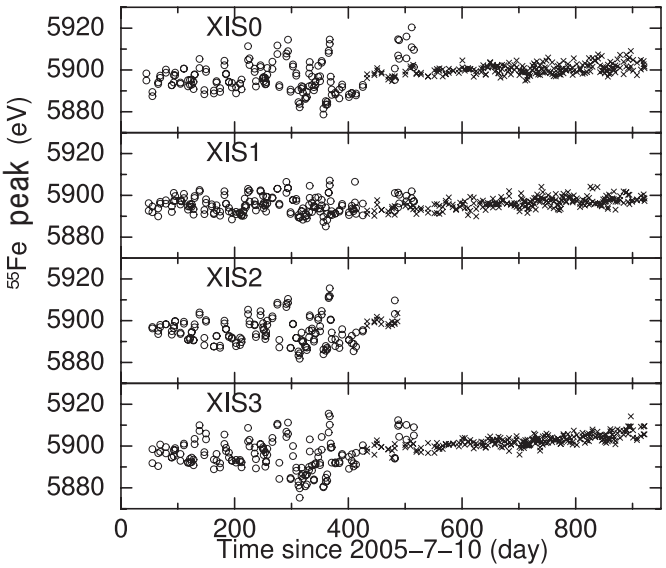

Figure 10. Time history of the center energy of the MnI Kα line for XIS 0-3 from the SCI-off (circle) and the SCI-on (cross) data. Each mark of the SCI-off data in the plot corresponds to an observation sequence whose effective exposure is more than 60 ksec. Each mark of the SCI-on data in the plot has an effective exposure of 150 ksec. The theoretical center energy of MnI Kα line is 5895 eV. Note that effective exposure time is different between the SCI-off data and the SCI-on data.

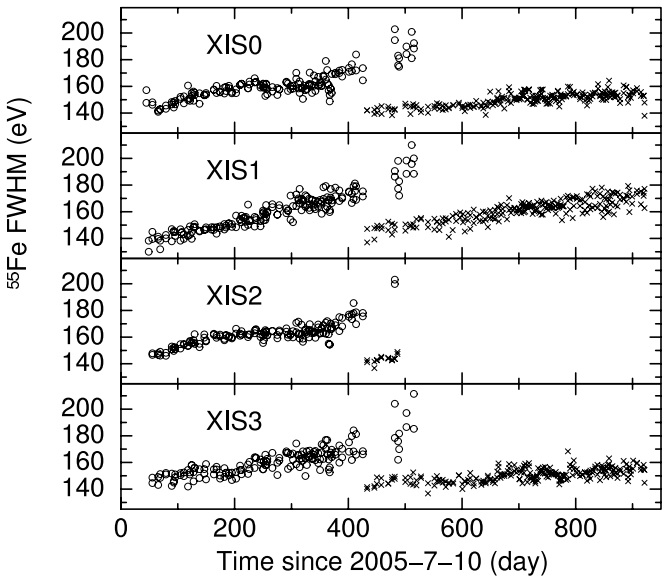

Figure 11. Time history of the energy resolution of MnI Kα line for XIS 0-3 from the SCI-off (circle) and the SCI-on (cross) data. Each mark of the SCI-off data in the plot corresponds to an observation sequence whose effective exposure is more than 60 ksec. Each mark of the SCI-on in the plot has an effective exposure of 150 ksec.

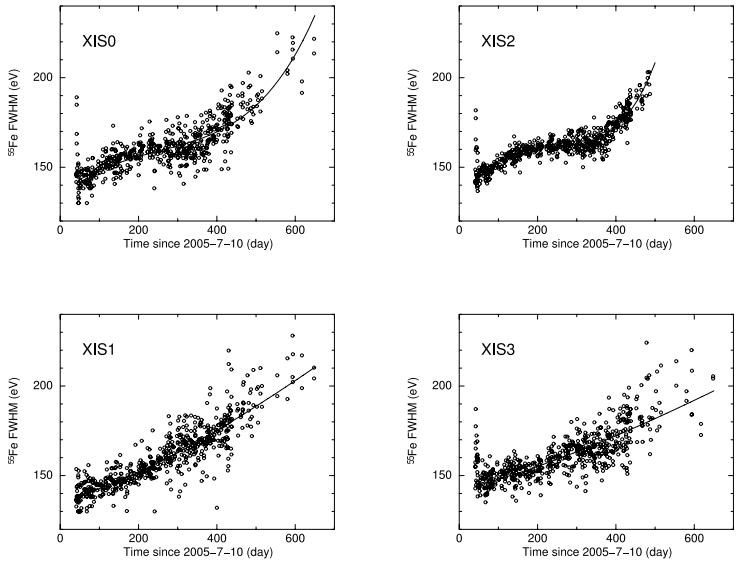

Figure 12. Energy resolution of the MnI Kα line for XIS 0-3 from the SCI-off data (open circles). The solid lines indicate the FWHM at 5895 eV which is incorporated in the redistribution matrix file (RMF). Each mark in the plot corresponds to an observation sequence.

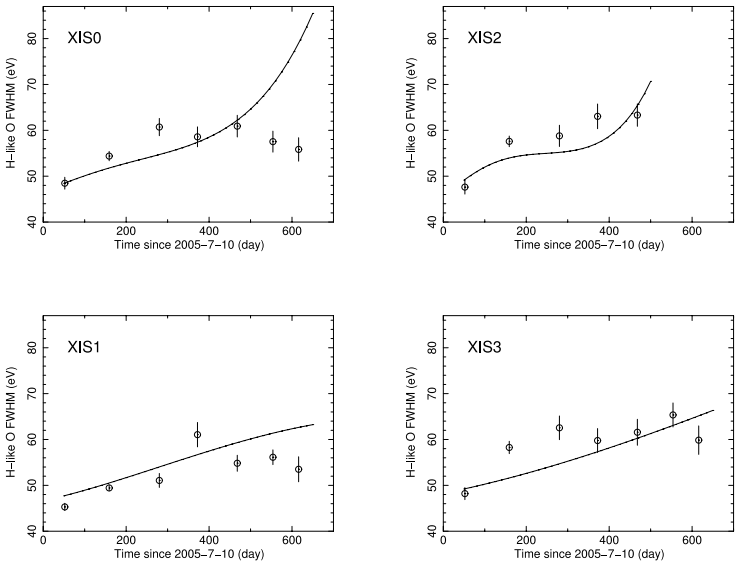

Figure 13. Energy resolution of OVIII Kα line for XIS 0-3 from the SCI-off data obtained in the E0102–27 observations (open circles). The solid lines indicate the FWHM at 653 eV which is incorporated in the RMF.

constant. The modeled FWHM at 5895 eV which is incorporated in the redistribution matrix file (RMF) and the energy resolution of the MnI Kα line are shown in figure 12. The modeled FWHM at 635 eV which is incorporated in the RMF and the energy resolution of the OVIII Kα line are shown in figure 13.

4. IN-ORBIT CALIBRATION OF SCI-ON DATA

4.1 CTI Correction Method for SCI Mode

A detailed description of the SCI-on technique is presented in Bautz et al. (2007)[8] and Uchiyama et al. (2007).[9] We briefly report the present calibration status. There are some differences in the CTI correction between the SCI-off data and the SCI-on data. First, in the SCI-on mode, we consider $f = 1$ for the FI sensors (XIS 0, 2, and 3) and 0.5 for the BI sensor (XIS 1) in the equation 2 and 3. Second, the CTI charge-dependent factor CTI_{POW} is different. It is a time constant value and different from segment to segment. The typical values are from 0.3 to 0.65. Finally, the CTI correction equation is different from that of the SCI-on data. We inject charge packets every 54 rows in the SCI-on mode, and the CTI value depends on the distance from the charge-injected row. Therefore, we modeled the CTI as a saw-tooth function. The details of the CTI correction for the SCI-on mode are described in Uchiyama et al. (2007)[9] and Bautz et al. (2007).[8]

4.2 Result of CTI Correction of SCI-on Data

Using "the saw-tooth function" defined in Uchiyama et al. (2007),[9] we performed the CTI correction. Then we performed the fine-tuning of the gain factor with the same procedure of the SCI-off mode which was mentioned in the section 3-3, using the data of ^{55}Fe and E0102–27.

After we corrected the CTI and the gain factor, we rechecked the energy gain. The time history of the energy gain of the MnI Kα line for XIS 0-3 from the SCI-off data is also shown in figure 10. The center energy of MnI Kα of the FI chips is higher than its theoretical value (5895 eV) systematically. Also there is a gradual increase of the gain. We will correct these trend in the future. The time history of the energy resolution of MnI Kα line for XIS 0-3 from the SCI-on data is shown in figure 11. By injecting charge packets periodically, energy resolution became significantly better. For example, the FWHM in September 2006 is 210 eV without the SCI, but it became 150 eV with the SCI and saw-tooth correction. This value is close to the resolution just after the launch (140 eV). In spite of the SCI, the resolution has been degrading gradually. This degradation is clearer in the BI chip.

5. DEGRADATION OF LOW ENERGY EFFICIENCY

The good low-energy response is an import feature of the XIS. However, we noticed the effective area below 2 keV has been decreasing with time after the launch. We consider it is most likely due to some contaminant stimulating on the surface of the XIS optical blocking filters (OBF).[7] In order to examine this efficiency, we have observed soft and stable sources, such as E0102–72, RXJ1856.5-3754, and the Cygnus loop, repeatedly, and monitored the value of the absorption of these objects. In figure 14, we show the on-axis thickness of the contaminant and an empirical model for the time evolution. We assume DEHP ($C_{24}H_{38}O_4$) as the contaminant.

6. SUMMARY

The Suzaku XIS performance for about two and a half years is summarized as follows:

1. With the column-to-column CTI correction obtained from the checker-flag CI experiments, the energy resolution (FWHM) of the MnI Kα line from the SCI-off data is improved to 173 eV on an average at the time of one year after the launch, while the resolution is 193 eV with the column-averaged CTI correction.
2. The energy gain of the SCI-off data is calibrated with an uncertainty of $\pm$ 0.7 % at $\sim$0.65 keV, and of $\pm$ 0.1 % at $\sim$5.9 keV.
3. The energy gain of the SCI-on data is systematically higher in the FI chips. Also it is increasing with the time. This trend will be corrected in the future.
4. The energy resolution (FWHM) of the MnI Kα line from the SCI-on data is improved from 210 eV to 150 eV at 5.9 keV in September 2006 with SCI and the CTI correction. In spite of the SCI, the energy resolution has been degrading gradually.

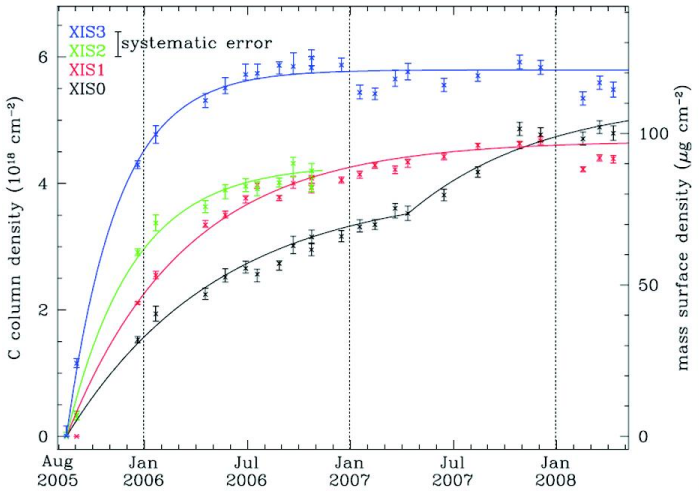

Figure 14. Time history of the on-axis thickness of the contaminant. Solid lines are empirical models of the time evolution of the thickness of the contaminant. We assume DEHP ($C_{24}H_{38}O_4$) as the contaminant.

ACKNOWLEDGMENTS

We thank all the Suzaku team members for their support of the observation and useful information on the XIS calibration. We thank Dr.Y.Ishisaki of Tokyo Metro University for his great contribution to the software development. M.O., H.U., and H.N. are supported by JSPS Research Fellowships for Young Scientists. This work is supported by the Grant-in-Aid for the 21st Century COE "Center for Diversity and Universality in Physics" from the Ministry of Education, Culture, Sports, Science and Technology (MEXT) of Japan.

REFERENCES

[1] Burke, B. E., Mountain. R. W., Daniels, P. J., Cooper, M. J., and Dolat, V. S., "CCD soft x-ray imagers for ASCA and AXAF," *Proc. SPIE* **2006**, pp. 272–285, 1993.

[2] Tomida, H., Matsumoto, H., Ozaki. M., Tazawa, Y., Awaki, H., Tsuru. T., Koyama, K., Tsunemi, H., and Yamamoto, K., "Radiation Damage on X-Ray CCDs and Restoration Technique for Space Astronomy," *PASJ* **49**, pp. 405–412, 1997.

[3] Prigozhin, G. Y., Burke, B. E., Bautz, M. W., Kissel. S. E., LaMarr, B., and Freytsis, M., "X-ray CCD with charge-injection structure," *Proc. SPIE* **5501**, pp. 357–365, 2004.

[4] Bautz, M. W., Kissel, S. E., Prigozhin, G. Y., LaMarr, B., Burke, B. E., and Gregory, J. A., "Progress in x-ray CCD sensor performance for the Astro-E2 X-ray imaging spectrometer," *Proc. SPIE* **5501**, pp. 111–122, 2004.

[5] LaMarr, B, Bautz, M. W., Kissel, S. E., Prigozhin, G. Y., Hayashida, K., Tsuru., T, and Matsumoto, H., "Ground calibration of X-ray CCD detectors with charge injection for the X-ray imaging spectrometer on Astro-E2," *Proc. SPIE* **5501**, pp. 385–391, 2004.

[6] Mitsuda, K. et al., "The X-ray observatory Suzaku," *PASJ* **59**, pp. 1–7, 2007.

[7] Koyama, K. et al., "X-ray imaging spectrometer (XIS) on Board Suzaku," *PASJ* **59**, pp. 23–33, 2007.

[8] Bautz, M. W. et al., "Mitigating CCD radiation damage with charge injection: first flight results from Suzaku," *Proc. SPIE* **6686**, 2007.

[9] Uchiyama, H. et al., "The onboard calibration for the spaced-row charge injection of the Suzaku XIS," *Proc. SPIE* **6686**, 2007.

[10] Nakajima, H. et al., "Performance of the Charge-Injection Capability of Suzaku XIS," *PASJ***60** ,pp. 1–10, 2008.